Metastable states from multinucleon excitations in ^{202}Tl and ^{203}Pb

S. G. Wahid,[1] S. K. Tandel,[1,*] Saket Suman,[1] M. Hemalatha,[2] Anurag Patel,[1] Poulomi Roy,[1] A. Y. Deo,[3] Pragati,[3] P. C. Srivastava,[3] Bharti Bhoy,[3] S. S. Bhattacharjee,[4] R. P. Singh,[4] S. Muralithar,[4] P. Chowdhury,[5] R. V. F. Janssens,[6,7] M. P. Carpenter,[8] T. L. Khoo,[8] F. G. Kondev,[8] T. Lauritsen,[8] C. J. Lister,[5,8] D. Seweryniak,[8] S. Zhu,[8,†] S. Rai,[9] and A. Sharma[10]

[1]*School of Physical Sciences, UM-DAE Centre for Excellence in Basic Sciences, University of Mumbai, Mumbai 400098, India*
[2]*Department of Physics, University of Mumbai, Mumbai 400098, India*
[3]*Department of Physics, Indian Institute of Technology Roorkee, Roorkee 247667, India*
[4]*Inter-University Accelerator Centre, Aruna Asaf Ali Marg, New Delhi 110067, India*
[5]*Department of Physics, University of Massachusetts Lowell, Lowell, Massachusetts 01854, USA*
[6]*Department of Physics and Astronomy, University of North Carolina at Chapel Hill, Chapel Hill, North Carolina 27599, USA*
[7]*Triangle Universities Nuclear Laboratory, Duke University, Durham, North Carolina 27708, USA*
[8]*Argonne National Laboratory, Argonne, Illinois 60439, USA*
[9]*Department of Physics, Visva-Bharati, Santiniketan 731235, India*
[10]*Himachal Pradesh University, Summer Hill Shimla, Shimla 171005, India*

(Received 10 February 2020; revised 10 July 2020; accepted 7 August 2020; published 24 August 2020)

The excited level structures of ^{202}Tl and ^{203}Pb, above the 7^+ and $29/2^-$ isomers, respectively, have been studied. An isomer with $I^\pi = 20^+$ and $T_{1/2} = 215(10)$ μs has been established in ^{202}Tl, and the level scheme extended from $I = 10$ to $20\,\hbar$ with the placement of fifteen new transitions. In ^{203}Pb, the $I^\pi = 37/2^+$ state is established to be metastable, with $T_{1/2} = 2.5(3)$ ns. Levels in both nuclei arise from intrinsic excitations, with likely particle-hole character for the higher-lying states in ^{203}Pb. The 20^+ isomer in ^{202}Tl is most likely associated with a $\pi h_{11/2}^{-1} \otimes \nu(i_{13/2}^{-2}, f_{5/2}^{-1})$ configuration, while the $37/2^+$ state in ^{203}Pb results from the excitation of five neutrons. Calculations, using both an empirical approach and the OXBASH code, have been performed to aid in the description of the excited level structure.

DOI: 10.1103/PhysRevC.102.024329

I. INTRODUCTION

Isotopes of Tl ($Z = 81$), with a one-proton hole with respect to magic $Z = 82$, and with neutron numbers approaching the shell closure at $N = 126$, exhibit evidence of metastable states built on intrinsic excitations. Such metastable states in the relatively neutron-rich isotopes $^{204–206}$Tl [1–3] have been well studied through multinucleon transfer reactions using ^{208}Pb beams or targets. In proton-rich isotopes with $A \leqslant 199$, prompt structures are known and there is no evidence of metastable states at high spin [4,5]. In contrast, there is comparatively limited information on metastable states in Tl isotopes with $A = 200$ to 203 [6–8]. Isotopes of Pb ($Z = 82$) with $A \approx 200$ have been studied more extensively and a number of isomers at low and intermediate spin identified [9]. Since most of them were populated in α-induced reactions, the available high-spin information is limited.

Information on isomeric states in the proximity of doubly-magic nuclei leads to insights into the relative ordering and precise spacing of single-neutron and proton energy levels, as these long-lived levels are usually built on intrinsic modes resulting from specific proton and/or neutron excitations. The structure of high-spin, metastable states is typically dominated by configurations involving high-j nucleons; in this case, those occupying the $\nu i_{13/2}$ and $\pi h_{11/2}$ subshells. Isomers at high excitation and spin have multinucleon configurations. In instances where the angular momentum available from neutron- and proton-hole configurations is exhausted, excitations across the $Z = 82$ and $N = 126$ shell gaps play a role in generating even higher spins. The precise excitation energies of isomers depend on the strength of residual interactions between the valence nucleons involved. Therefore, establishing such states provides this additional insight. Systematic data on isomers across isotopic or isotonic chains allows for discriminating tests of the validity of modern-day shell-model calculations and of the various interactions used. While high-spin isomers have recently been studied in some Hg, Tl, and Pb isotopes [9,10], there is limited information on some nuclei in these isotopic chains which cannot be accessed readily through heavy-ion induced fusion-evaporation reactions or those which cannot be populated using inelastic excitation or few-nucleon transfer reactions.

*Corresponding author: sujit.tandel@cbs.ac.in, sktandel@gmail.com
†Present address: National Nuclear Data Centre, Brookhaven National Laboratory, Upton, New York 11973-5000, USA.

II. EXPERIMENT AND DATA ANALYSIS

The excited level structure of ^{202}Tl was determined from two experiments: one using the INGA spectrometer (Indian National Gamma Array) [11], and the other with the Gammasphere array [12,13]. The experiment using INGA was performed at the Inter-University Accelerator Centre (IUAC), New Delhi, India. Excited levels in ^{202}Tl were populated through the ^{198}Pt(^{7}Li, $3n$) fusion-evaporation reaction at incident energies of 31–36 MeV with the ^{7}Li beam obtained from the Pelletron accelerator. The ^{198}Pt target was isotopically enriched (≈92%) and had a thickness ≈10 mg/cm^2. The INGA array, at the time of the experiment, consisted of 14 Compton-suppressed clover HPGe (high-purity germanium) detectors and a planar HPGe one. The directional correlation from oriented nuclei (DCO) method [14,15] was used to determine the multipole order of transitions observed in the INGA experiment, since the feeding from the high-spin isomer was almost insignificant (see below). Data obtained with the clover detectors placed at 90°allowed for the deduction of the IPDCO (integrated polarization from direction correlation) ratios [16] instrumental in the assignment of either electric or magnetic character to transitions of interest. The planar detector enabled the efficient detection of low-energy ($\leqslant$100 keV) γ rays. Two- and higher-fold γ-ray coincidence events were recorded in the experiment with the INGA array.

The second experiment was performed at the Argonne National Laboratory with a 1450-MeV ^{209}Bi beam from the ATLAS accelerator incident on a 50 mg/cm^2 ^{197}Au target. The nuclei of interest were populated through multinucleon transfer reactions. Gammasphere was composed of 100 Compton-suppressed HPGe detectors. Three- and higher-fold coincidence events were recorded in this measurement. While a coincidence time window of ≈1 μs was employed in both experiments, an additional beam pulsing, with a 200 μs on and 800 μs off period, was utilized during part of the Gammasphere experiment. This enabled a search for long-lived isomers. Two- and higher-fold coincidence data were collected in the 800 μs beam-off period.

Complementary information obtained from the two experiments was crucial in establishing the level scheme of ^{202}Tl. A number of histograms of different types were created to aid in establishing the level ordering, the half-lives of isomers, and the multipole order and character of transitions. Two- and three-dimensional symmetric energy histograms, asymmetric ones for DCO and IPDCO analysis, and one with the planar versus all clover detectors, were created using the data from the INGA experiment. The Gammasphere data were utilized to create three-dimensional symmetric energy histograms to inspect coincidence relationships between γ rays in the prompt time range (±50 ns with respect to when the beam was incident on the target) and in the delayed regime (+50 to +650 ns). In the case of γ rays detected during the 800 μs beam-off period, coincidence histograms with a prompt time condition between those photons in a given event (±50 ns with respect to each other) were required. Additionally, energy-gated two-dimensional energy versus time difference histograms were also created for the determination of half-lives within the coincidence window [17–19]. The symmetric energy histograms were analyzed using the RADWARE suite of programs [20].

III. RESULTS

A. ^{202}Tl

The $N = 121$ isotones ^{202}Tl and ^{203}Pb had been previously studied using ^{204}Pb$(d,\alpha)^{202}$Tl [21], ^{203}Tl$(n,2n)^{202}$Tl [22], and ^{202}Hg$(\alpha,3n)^{203}$Pb [9] reactions. Experimental information on ^{202}Tl was limited to states up to the $I^\pi = 9^+$ level at $E_x = 2340$ keV. In the present work, the decay scheme of ^{202}Tl has been considerably extended with the inclusion of fifteen new transitions up to the $I^\pi = 20^+$ level at $E_x =$ 4148 keV. Furthermore, a new isomer with $I^\pi = 20^+$ and $T_{1/2} = 215(10)$ μs has been identified.

The 7^+ states in doubly-odd Tl isotopes of the $A \approx$ 190–200 region have isomeric character. Such a state with $T_{1/2} = 591(3)$ μs had been previously identified in ^{202}Tl; the half-life is confirmed in the present work. The 12^- states in ^{202,204,206}Tl had been first established using ^{204,206,208}Pb(d,α) reactions [21] and had been located at $E_x = 2.15$, 2.31, and

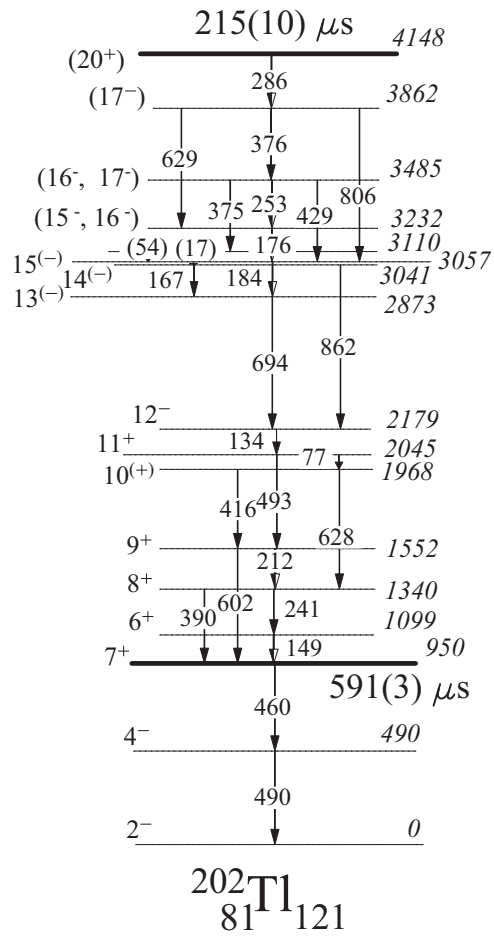

FIG. 1. Partial decay scheme of ^{202}Tl established from the present work. The transitions above the 10^+ level are all newly identified. The isomer with $I^\pi = 20^+$ is newly determined from the present work while the one with $I^\pi = 7^+$ had been established previously [22].

TABLE I. Energies and intensities of γ rays, and excitation energies and spin-parities of initial and final states in ^{202}Tl. Transition energies are accurate to within 0.5 keV. Statistical uncertainities on γ-ray intensities and DCO ratios are listed. DCO and IPDCO ratios are from the INGA data and relative intensities are from the delayed regime in the Gammasphere experiment. Typical values of DCO ratios in a gate on a stretched dipole transition were found to be ≈1.0 and 2.0 for known stretched dipole and quadrupole γ rays, respectively. Multipolarity assignments from the present work are included. "#" indicates multipolarity assignment from intensity balance considerations listed in Table II. "∗" indicates multipolarity assignment based on DCO and IPDCO ratios.

E_γ (keV)	E_i (keV) → E_f (keV)	$I_i^\pi \rightarrow I_f^\pi$	I_γ	DCO	IPDCO	Multipolarity
(17)	3057 → 3041	$15^{(-)} \rightarrow 14^{(-)}$				
(54)	3110 → 3057	$\rightarrow 15^{(-)}$				
77.0	2045 → 1968	$11^+ \rightarrow 10^{(+)}$				
134.2	2179 → 2045	$12^- \rightarrow 11^+$	139(6)	1.15(6)		$E1^\#$
149.2	1099 → 950	$6^+ \rightarrow 7^+$	5(1)			
166.7	3041 → 2873	$14^{(-)} \rightarrow 13^{(-)}$	8(1)			$M1^\#$
175.6	3232 → 3057	$(15^-, 16^-) \rightarrow 15^{(-)}$	34(4)			$M1^\#$
183.6	3057 → 2873	$15^{(-)} \rightarrow 13^{(-)}$	38(4)			$E2^\#$
211.6	1552 → 1340	$9^+ \rightarrow 8^+$	50(3)	0.95(5)		$M1^\#$
240.6	1340 → 1099	$8^+ \rightarrow 6^+$	15(2)	1.76(16)		
253.0	3485 → 3232	$(16^-, 17^-) \rightarrow (15^-, 16^-)$	64(4)			$E2^\#$
285.8	4148 → 3862	$(20^+) \rightarrow (17^-)$	102(9)			$E3^\#$
375.0	3485 → 3110	$(16^-, 17^-) \rightarrow$	13(3)			
376.5	3862 → 3485	$(17^-) \rightarrow (16^-, 17^-)$	97(7)			$M1^\#$
389.5	1340 → 950	$8^+ \rightarrow 7^+$	114(5)		−0.062(4)	
416.0	1968 → 1552	$10^{(+)} \rightarrow 9^+$	9(1)			
429.0	3485 → 3057	$(16^-, 17^-) \rightarrow 15^{(-)}$	12(3)			
492.7	2045 → 1552	$11^+ \rightarrow 9^+$	134(6)	1.66(6)	0.045(6)	$E2^*$
601.8	1552 → 950	$9^+ \rightarrow 7^+$	48(4)	1.87(13)		
628.4	1968 → 1340	$10^{(+)} \rightarrow 8^+$	49(4)	1.65(10)		
629.0	3862 → 3232	$(17^-) \rightarrow (15^-, 16^-)$	17(3)			
694.3	2873 → 2179	$13^{(-)} \rightarrow 12^-$	80(8)	1.20(7)		
806.2	3862 → 3057	$(17^-) \rightarrow 15^{(-)}$	54(7)			
861.7	3041 → 2179	$14^{(-)} \rightarrow 12^-$	100(9)	1.73(11)		

2.61 MeV, respectively. With subsequent, high-resolution γ-ray measurements, the excitation energies of these levels in ^{204,206}Tl were determined to be 2319 and 2643 keV, respectively, and their isomeric character was established with $T_{1/2} = 2.6$ μs and 3.74 min, respectively. However, a similar level has not been identified in ^{200}Tl [6,23,24]. In ^{202}Tl, a 12^- state is identified at $E_x = 2179$ keV from the present work, a value within the uncertainty reported from the earlier (d, α) measurement. The situation is similar to that encountered in ^{206}Tl, where the deviation is ≈30 keV. The half-life of this level is less than 2 ns, based on the lack of discernible centroid shift in time spectra between γ rays feeding and deexciting it, when compared to such spectra for prompt transitions with similar energies.

The level scheme for ^{202}Tl determined from the present work is illustrated in Fig. 1, and detailed numerical data are presented in Table I. The γ rays assigned to ^{202}Tl are clearly evident in the data from the INGA experiment in single coincidence gates on the 134-, 694-, and 862-keV transitions (Fig. 2). Double-gated coincidence spectra, in the delayed regime, from the Gammasphere experiment, are presented in Figs. 3 and 4. In Fig. 3, gates are placed on the 390-, 493-, 602-, and 628-keV transitions which had been previously established. Double coincidence gates on the 493-keV transition with the newly identified 134-, 694-, and 862-keV γ rays are displayed in Fig. 4. The 286-keV γ ray, which is barely visible in the prompt data of Fig. 2, is most prominent in the delayed spectra, thereby affirming its character as an isomeric

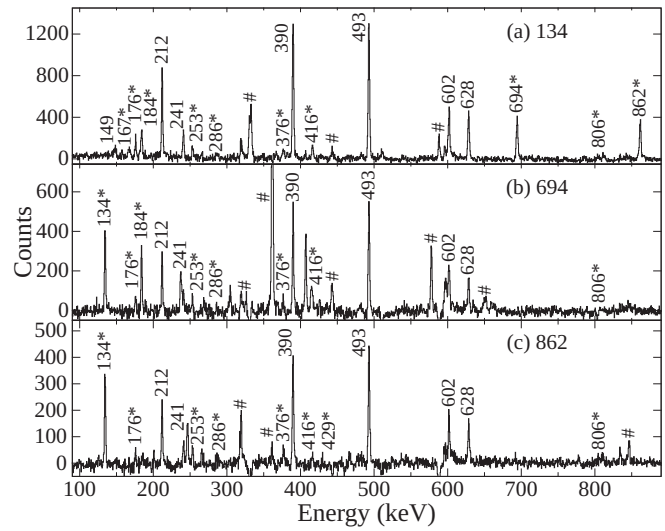

FIG. 2. Sample coincidence spectra obtained from the INGA experiment with gates on the 134-, 694-, and 862-keV transitions in ^{202}Tl. Newly identified γ rays are marked with asterisks, while contaminant ones are presented with hash marks.

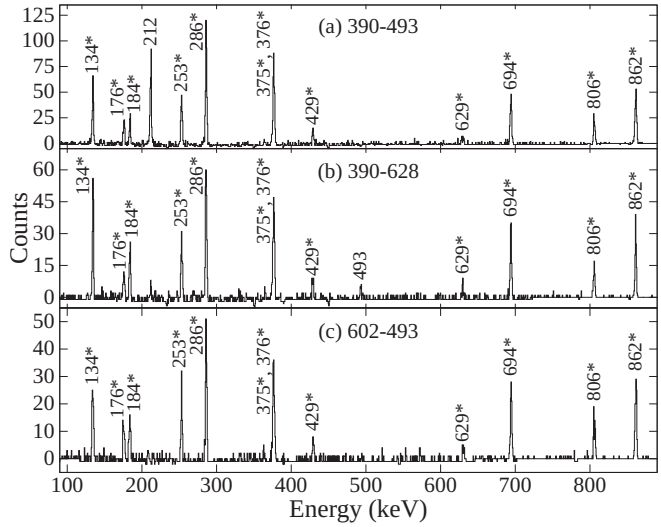

FIG. 3. Double-gated coincidence spectra with γ rays detected in the delayed regime during the Gammasphere experiment. Gates are placed on previously established transitions in ^{202}Tl. Newly identified γ rays are marked with asterisks.

transition at high spin. The coincidence spectra in Fig. 5, along with others, allow for the clear identification and placement of all transitions, including those which are closely spaced in energy (e.g., the 628-629 keV and 375-376 keV doublets).

The presence of a 77-keV transition is inferred from the data in the planar HPGe detector, when recorded in coincidence with γ rays observed in the clover HPGe detectors during the INGA experiment (Fig. 6). Since target and evaporation residue (Pt and Tl, respectively) x rays lie in the 65–85 keV range, γ rays in this same region may not be easily visible. Based on the intensity flow, it was first determined that a previously unobserved low-energy γ ray possibly feeds the 10^+ level at $E_x = 1968$ keV, a state primarily deexcited

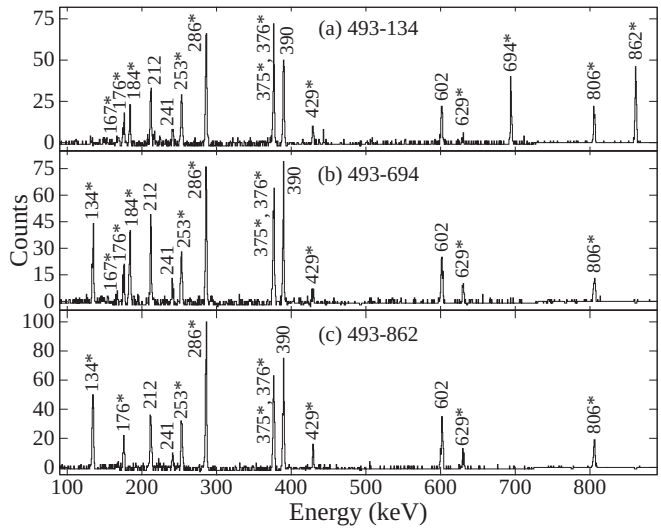

FIG. 4. Same as Fig. 3, with gates on the previously identified 493-keV γ ray and newly established ones in ^{202}Tl. Transitions identified in the present work are indicated by asterisks.

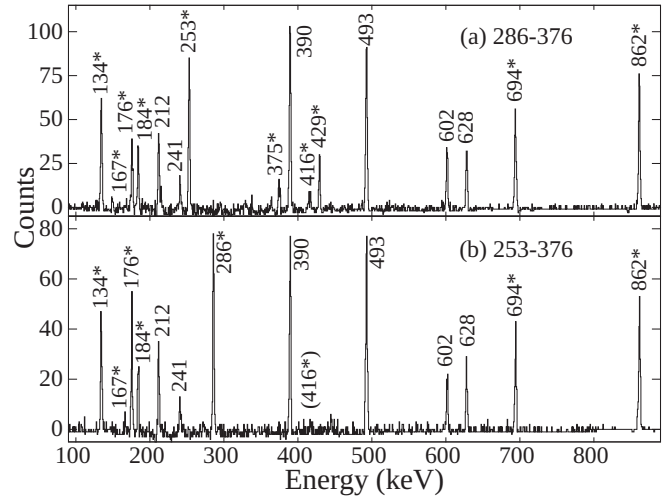

FIG. 5. Same as Fig. 3, with gates on newly identified high-spin transitions in ^{202}Tl. Transitions identified in the present work are given with asterisks.

by the 628-keV transition. Since the 493-keV γ ray deexcites the 11^+ state, which lies above the 10^+ level, it would not be in coincidence with a γ ray feeding this state. However, the 628-keV transition is expected to be in strong coincidence with such a low-energy γ ray. Figure 6 illustrates coincidence spectra observed in the planar HPGe counter with gates placed on γ rays in the clover HPGe detectors. It is evident that Pt and Tl K x rays dominate the total projection spectrum [Fig. 6(a)] in the 65–85 keV region. In order to subtract contributions from the target (Pt) x rays, a normalized subtraction was performed of the spectrum of Pt x rays visible in the total projection spectrum from the gates on the 493- and 628-keV transitions [Figs. 6(b) and 6(c)]. Consequently, there is little or no evidence for Pt x rays in Figs. 6(b) and 6(c). However, as expected, Tl x rays remain visible. It is noteworthy that a clear peak is now visible at 77 keV in Fig. 6(c), in contrast to Fig. 6(b). This stark difference allows the assignment of the observed 77-keV γ ray in Fig. 6(c) to the deexcitation of the $I^\pi = 11^+$, $E_x = 2045$-keV level. It may be noted that this state is also independently established from the decay of the strong, 493-keV transition. It is relevant to mention here that, following the normalized subtraction of Pt x rays, the 212-keV γ ray is clearly seen to be coincident with the 493-keV line, but not with the 628-keV transition, consistent with the proposed decay scheme. The observed intensity of the 77-keV γ ray is consistent with an $M1$ rather than an $E1$ character, with theoretical total conversion coefficients of 3.37 and 0.18, respectively [25]. This assignment is in agreement as well with the unambiguous evidence of an electric quadrupole character for the 493-keV transition from DCO and IPDCO ratios [Figs. 7(a) and 7(b)]. The gating transition for obtaining the DCO ratios in Fig. 7(a) had dipole nature; values of $\approx$1 and 2 correspond to dipole and quadrupole character, respectively.

From the INGA experiment, IPDCO ratios could be obtained for the 390- and 493-keV γ rays. The magnetic character of the 390-keV transition is confirmed, while an electric

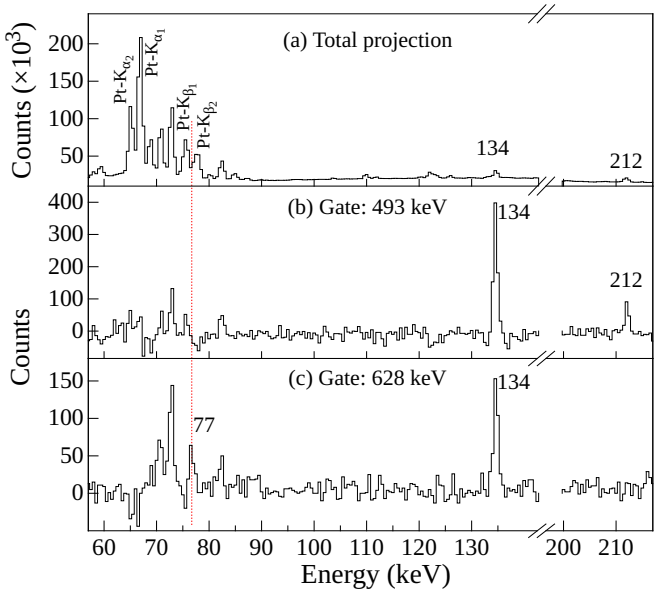

FIG. 6. Spectra from the planar HPGe detector in the INGA experiment illustrating the newly identified 77-keV transition in ^{202}Tl. Details are provided in the text.

nature is inferred for the 493-keV γ ray [Fig. 7(a)]. The DCO ratios obtained from the INGA experiment [Fig. 7(b)] confirm the previously assigned multipole orders for the 212-, 241-, 390-, 602-, and 628-keV γ rays. The 602-keV transition had been previously assigned $M1 + E2$ character. From the present work, a DCO ratio of 1.87(13) has been determined with a gate on a dipole transition, indicating quadrupole character for the 602-keV γ ray. Consequently, since the 602-keV γ ray deexcites to the 7^+ state at 950 keV, the spin of the 1552-keV level is reassigned to $I^\pi = 9^+$, different from the previous 8^+ assignment. The multipole orders assigned to the above transitions based on DCO ratios [Fig. 7(a)] are 212 (dipole), 241 (quadrupole), 390 (dipole), and 628 (quadrupole), with the IPDCO ratio for the 390-keV γ ray indicating magnetic character [Fig. 7(b)]. Out of the newly identified transitions, the multipole order of the following ones could be ascertained: 134 (dipole), 694 (dipole), and 862 (quadrupole) keV. More details on DCO and IPDCO ratios for ^{202}Tl, obtained from the INGA experiment, may be found in Table I. Though the lack of statistics prevented the unambiguous determination of DCO ratios for other transitions, intensity balance considerations were used for the assignment of multipolarity to several γ rays using data collected in the 800 μs beam-off period with Gammasphere, as practically all the feeding was found to originate from the $T_{1/2} = 215(10)$ μs isomer at $E_x = 4148$ keV. The multipolarities determined for various transitions in this manner are listed in Table II. A few notable examples are the 134-keV γ ray, feeding the 11^+ level, for which an $E1$ character is deduced that leads to the 12^- assignment for the $E_x = 2179$ keV level. The $E1$ assignment for the 134-keV transition follows from the balance of intensity feeding and deexciting the 2179-keV level (Table II). The intensity feeding into this level through the 694- and 862-keV γ rays with most likely $M1$ and $E2$ character, respectively, is balanced with that deexciting via the 134-keV transition. Given the relatively high energy of the 694- and 862-keV γ rays, the total intensity of these transitions inferred from the respective γ-ray intensities is not very sensitive to the choice of multipolarity since the conversion coefficients for all reasonably probable multipolarities are small. On the other hand, the total intensity of the 134-keV transition inferred from the γ-ray intensity would be quite different for the possible $E1$, $M1$, and $E2$ multipolarities. Clearly, only $E1$ multipolarity for the 134-keV transition is allowed from intensity balance considerations (Table II) and others are excluded. Similar arguments allow for both $M1$ and $E2$ multipolarities for the 167-keV γ ray (Table II). The $M1$ assignment is preferred since $E2$ multipolarity would lead to $I^\pi = 15^-$ for the 3041-keV level, and a consequent, unphysical $M3$ character for the 862-keV transition deexciting this level. For the case of the isomeric, 286-keV transition, an $E3$ multipolarity is deduced leading to a $I^\pi = 20^+$ assignment for the isomer at $E_x = 4148$ keV. The half-life of this state has been deduced by fitting the time distribution of the intensities of different γ rays in the 800 μs beam-off period (Fig. 8). A value of $T_{1/2} = 215(10)$ μs is inferred from the weighted average of half-lives obtained by fitting the time distributions of the 134-, 176-, 253-, 286-, 376-, 390-, and 493-keV γ rays.

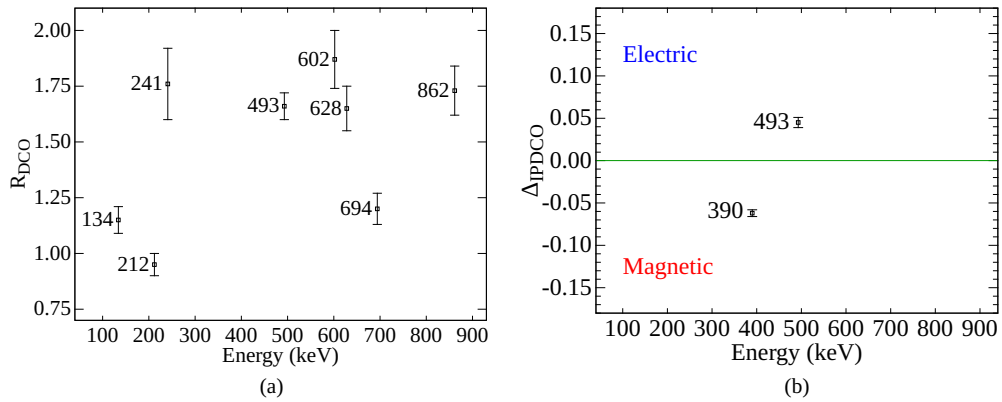

FIG. 7. DCO and IPDCO ratios for selected transitions in ^{202}Tl as obtained from the INGA experiment; see text for details.

TABLE II. Multipolarity assignments for transitions in ^{202}Tl based on intensity balance arguments. The total intensities feeding and deexciting a given level populated in the delayed regime from the decay of the $T_{1/2} = 215(10)$ μs isomer, populated in the Gammasphere experiment, have been considered. Theoretical conversion coefficients [25] have been used. For relatively high-energy transitions ($\geqslant$600 keV), the choice of multipolarity does not significantly affect the value of the total intensity of the relevant transition. In the case of lower-energy, weak transitions, the choice of multipolarity does not significantly alter the sum of intensities either. The procedure has been used to assign multipolarity to transitions with relatively low energy ($\approx$100–300 keV) which may have significant conversion coefficients. Gating transitions appropriate for the determination of the intensity balance for each level have been used. The multipolarities (and corresponding intensities) indicated in boldface are the ones established from the data. Level and γ-ray energies, relative intensities, multipolarities, theoretical conversion coefficients, total intensities, and sums of feeding and deexciting intensities are listed. Sum*: I_{total} (feeding). Sum$^\#$: I_{total}(deexciting).

E_x (keV)	E_γ (keV)	I_γ	Multipolarity	α_t	I_{total}	Sum*	Sum$^\#$
1552	416*	9(1)	***M*1**	0.1622	**10(2)**	**148(6)**	
	493*	134(6)	***E*2**	0.0291	**138(6)**		
	212$^\#$	50(3)	*E*1	0.0658	53(3)		73(4)
			***M*1**	1.0220	**101(6)**		**150(7)**
			*E*2	0.3347	67(4)		83(4)
	602$^\#$	48(4)	***E*2**	0.0182	**49(4)**		
2179	694*	80(8)	***M*1**	0.0422	**83(8)**	**184(12)**	
	862*	100(9)	***E*2**	0.0085	**101(9)**		
	134$^\#$	139(6)	***E*1**	0.2070	**168(8)**		**168(8)**
			*M*1	3.7300	657(17)		657(26)
			*E*2	1.7900	387(10)		387(15)
2873	**167***	8(1)	*E*1	0.1190	9(1)		
			***M*1**	1.9960	**24(2)**		
			*E*2	0.7768	15(1)		
	184*	38(4)	*E*1	0.0934	42(4)		
			*M*1	1.5200	97(10)		
			***E*2**	0.5470	**60(6)**	**84(6)**	
	694$^\#$	80(8)	***M*1**	0.0422	**83(8)**		**83(8)**
3057	**176***	34(4)	*E*1	0.1044	38(4)	123(9)	
			***M*1**	1.7220	**93(11)**	**178(14)**	
			*E*2	0.6420	56(6)	141(10)	
	375*	13(3)	*E*1	0.0171	13(3)		
			***M*1**	0.2130	**16(3)**		
			*E*2	0.0583	14(3)		
	429*	12(3)	*E*1	0.0128	12(3)		
			***M*1**	0.1494	**14(3)**		
			*E*2	0.0412	13(3)		
	806*	54(7)	*E*1	0.0036	55(7)		
			*M*1	0.0286	56(7)		
			***E*2**	0.0098	**55(7)**		
	694$^\#$	80(8)	***M*1**	0.0422	**83(8)**		**184(12)**
	862$^\#$	100(9)	***E*2**	0.0085	**101(9)**		
3232	**253***	64(4)	*E*1	0.0429	67(4)	85(6)	
			*M*1	0.6260	104(6)	122(7)	
			***E*2**	0.1870	**76(5)**	**94(6)**	
	629*	17(3)	*E*1	0.0058	17(3)		
			M1	0.0543	**18(4)**		
			*E*2	0.0165	17(4)		
	176$^\#$	34(4)	***M*1**	1.7220	**93(11)**		**93(11)**
3862	**376***	97(7)	*E*1	0.0171	98(7)	171(11)	
			***M*1**	0.2130	**117(9)**	**190(12)**	
			*E*2	0.0583	102(8)	175(11)	
	629*	17(3)	*E*1	0.0057	17(3)		
			***M*1**	0.0543	**18(4)**		
			*E*2	0.0165	17(4)		
	806*	54(7)	*E*1	0.0036	55(7)		
			*M*1	0.0286	56(7)		
			***E*2**	0.0098	**55(7)**		

TABLE II. (*Continued.*)

E_x (keV)	E_γ (keV)	i_γ	Multipolarity	α_t	i_{total}	Sum*	Sum#
	694#	80(8)	***M*1**	0.0422	**83(8)**		**184(12)**
	862#	100(9)	***E*2**	0.0085	**101(9)**		
4148	**286***	102(9)	*E*1	0.0320	106(9)	106(9)	
			*M*1	0.4470	148(13)	148(13)	
			*E*2	0.1280	116(10)	116(10)	
			*M*2	1.7320	280(25)	280(25)	
			***E*3**	0.7240	**177(16)**	**177(16)**	
	694#	80(8)	***M*1**	0.0422	83(8)		**184(12)**
	862#	100(9)	***E*2**	0.0085	101(9)		

B. ^{203}Pb

In ^{203}Pb, states up to the $I^\pi = 37/2^+$ level at $E_x = 5026$ keV had been previously established [9]. From the present work, isomeric character was inferred for this $I^\pi = 37/2^+$ state, and in addition, the level scheme was extended up to $E_x = 6701$ keV (Fig. 9 and Table III). Representative double-gated coincidence spectra are displayed in Fig. 10. The half-life of the $I^\pi = 37/2^+$ level has been deduced using the centroid-shift method [26]. The time difference between the 568- and 1529-keV γ rays located below and above this state is histogrammed and compared with that of two prompt transitions with similar energies. A value of $T_{1/2} = 2.5(3)$ ns is inferred (Fig. 11). With a gate on a quadrupole transition, a DCO ratio of 0.86(8) was obtained for the 1529-keV γ ray. This is suggestive of its quadrupole character leading to an $I = 41/2$ assignment for the 6554-keV level. For the 1056-keV transition, dipole character is tentatively indicated, however, a firm conclusion is not possible, based on the available information.

IV. DISCUSSION

A. Isomeric states and configurations in ^{202}Tl

The doubly-odd isotope ^{202}Tl ($Z = 81$, $N = 121$) appears to be nearly spherical as it does not exhibit the weakly collective, oblate structures arising from the occupation of the $h_{9/2}$ proton orbital (from across the $Z = 82$ shell gap) that are evident in Tl isotopes with $A \leqslant 201$ [4–6,8]. Rather, the ^{202}Tl excited states appear to be associated with intrinsic excitations. Metastable 7^+ states are observed in doubly-odd Tl isotopes ranging from the proton-rich ($A \approx 190$) to the neutron-rich ($A = 206$) region. Their half-lives have been measured to range from nanoseconds to hours [27–32]. In addition, magnetic moments have been measured for most of these states, and these support a $(\pi s_{1/2}^{-1} \otimes \nu i_{13/2}^{-1})$ assignment. Furthermore, the energy systematics of these 7^+ isomers, in terms of a gradual progression from lower to higher excitation energy with increasing mass number [27–32], also supports the presence of the $i_{13/2}$ neutron in their configuration, as the neutron Fermi level moves higher in energy with mass number A, and farther away from the $i_{13/2}$ orbital (Fig. 12).

Weakly collective, oblate-deformed, negative-parity structures built on 7^- or 8^- bandheads have been established in

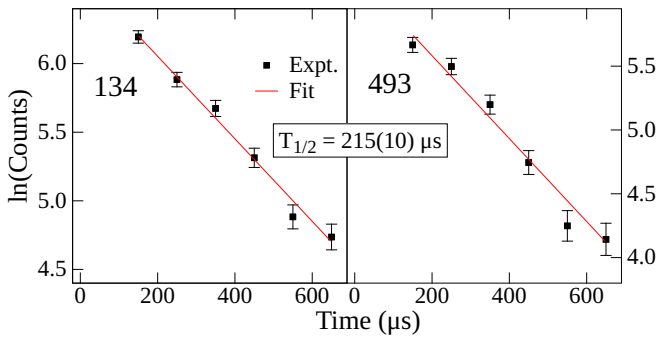

FIG. 8. Time distribution of coincidence counts for the 134- and 493-keV γ rays in ^{202}Tl from the Gammasphere experiment. All high-spin transitions are fed by the $I^\pi = 20^+$ isomer for which $T_{1/2} = 215(10)$ μs is deduced.

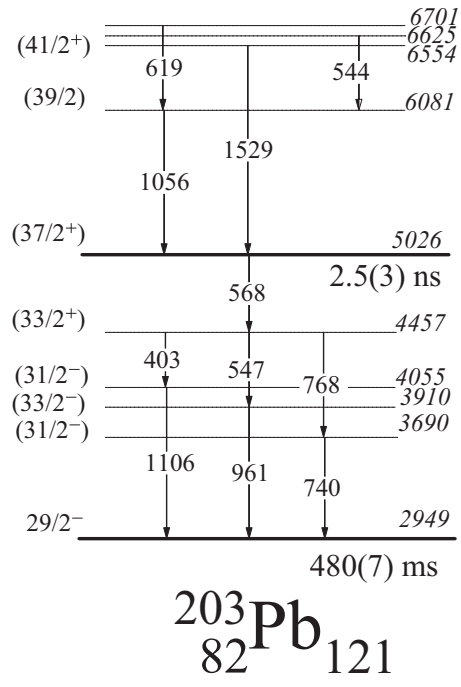

FIG. 9. Partial decay scheme of ^{203}Pb above the 480-ms isomer. Transitions above the $37/2^+$ level, for which isomeric character is established from the present work, are newly identified. The isomeric, $29/2^-$ level had been previously established [9].

TABLE III. Energies and intensities of γ rays, and excitation energies and spin-parities of initial and final states in ^{203}Pb. Transition energies are accurate to within 0.5 keV. Typical values of DCO ratios in a gate on a stretched quadrupole transition were found to be ≈ 0.5 and 1.0 for known stretched dipole and quadrupole γ rays, respectively. Statistical uncertainties on γ-ray intensities and DCO ratios are included.

E_γ (keV)	E_i (keV) $\rightarrow$ E_f (keV)	$I_i^\pi \rightarrow I_f^\pi$	I_γ	DCO
402.6	4457 $\rightarrow$ 4055	$(33/2^+) \rightarrow (31/2^-)$	41(2)	0.62(4)
544.2	6625 $\rightarrow$ 6081	$\rightarrow (39/2)$	14(1)	
546.7	4457 $\rightarrow$ 3910	$(33/2^+) \rightarrow (33/2^-)$	40(2)	
568.1	5026 $\rightarrow$ 4457	$(37/2^+) \rightarrow (33/2^+)$	100(3)	
619.4	6701 $\rightarrow$ 6081	$\rightarrow (39/2)$	32(2)	
740.5	3690 $\rightarrow$ 2949	$(31/2^-) \rightarrow 29/2^-$	26(1)	0.64(6)
767.8	4457 $\rightarrow$ 3690	$(33/2^+) \rightarrow (31/2^-)$	20(1)	
961.0	3910 $\rightarrow$ 2949	$(33/2^-) \rightarrow 29/2^-$	29(2)	1.05(9)
1055.7	6081 $\rightarrow$ 5026	$(39/2) \rightarrow (37/2^+)$	26(1)	
1105.6	4055 $\rightarrow$ 2949	$(31/2^-) \rightarrow 29/2^-$	33(2)	
1528.7	6554 $\rightarrow$ 5026	$(41/2) \rightarrow (37/2^+)$	29(2)	0.86(8)

doubly-odd, $A \leqslant 200$ isotopes [5,6]. These states have an underlying $(\pi h_{9/2} \otimes \nu i_{13/2}^{-1})$ configuration. As the nuclear shape becomes nearly spherical for $A \geqslant 202$ isotopes of Tl, the excitation to the $h_{9/2}$ orbital across the $Z = 82$ gap becomes energetically more expensive. In contrast, excitations involving the $h_{11/2}$ orbital below $Z = 82$ are favored, in particular the $(\pi h_{11/2}^{-1} \otimes \nu i_{13/2}^{-1})$ configuration resulting in a 12^- state. Such a 12^- level is established to be isomeric with $T_{1/2} = 2.6(2)$ μs and 3.74(3) min in ^{204}Tl and ^{206}Tl, respectively [1,3]. In the present work, the 12^- state is newly established; however, it is not of isomeric character. Possible reasons for this absence of isomerism will be discussed hereafter. The 12^- states in ^{202,204,206}Tl had been previously populated in (d, α) reactions using Pb targets, and the angular momentum of excited states in these isotopes had been determined through angular distribution measurements of the outgoing α particles. The associated excitation energies in ^{202,204,206}Tl had been determined to be 2.15, 2.31, and 2.61 MeV, respectively [21]. Due to the inherent, significantly larger uncertainties in particle spectroscopy (in this case, a few tens of keV) in comparison to the precision that can be achieved in γ-ray measurements with HPGe detectors (a fraction of a keV), the excitation energies of these 12^- states were not precisely determined in the earlier studies. Subsequent γ-ray measurements have established the 12^- states in ^{204}Tl and ^{206}Tl to be located at 2319 and 2643 keV, respectively [1,3]. In the latter case, the 12^- energy had been underestimated by $\approx$30 keV in the (d, α) measurement. For ^{202}Tl, a similar difference is evident: 2.15 MeV from the (d, α) study versus 2179 keV from the present work. Additionally, it may be noted that the 140-keV difference in the excitation energies of the 12^- states in ^{202}Tl and ^{204}Tl derived from experiment matches quite well with the 178-keV difference in the one-neutron, $i_{13/2}$ energies obtained from an average of the energies in the corresponding

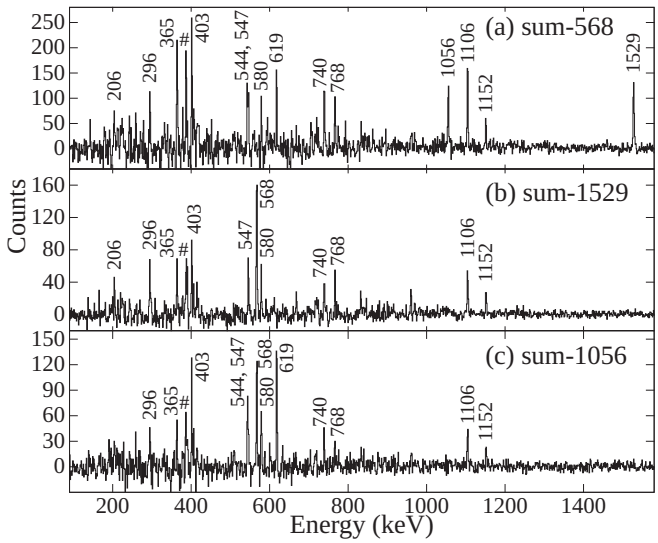

FIG. 10. Double-gated coincidence spectra displaying transitions in ^{203}Pb. Summed gates, including γ rays above the $29/2^-$ isomer and below the 568-keV transition are used. Some of the newly identified γ rays visible in the spectra, though clearly associated with ^{203}Pb (206, 296, 365, 580, 1152, and 1460 keV), could not be placed in the level scheme, most likely due to the presence of multiple low-energy γ rays which could not be observed in the present work. Contaminant transitions are indicated with hash marks.

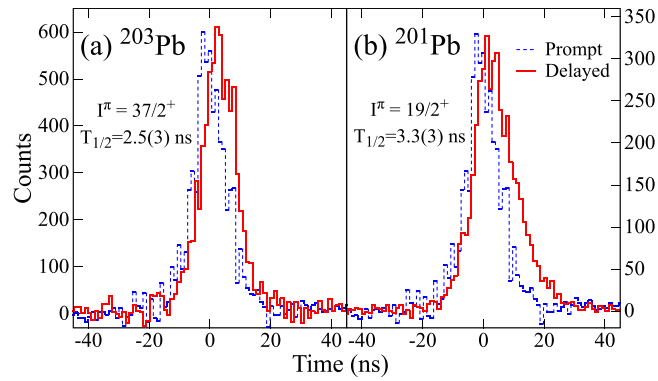

FIG. 11. Half-life of the $I^\pi = 37/2^+$ state in ^{203}Pb determined using the centroid-shift method. For comparison, the half-life of the $I^\pi = 19/2^+$ state in ^{201}Pb, also populated in this experiment, is illustrated; the extracted value of 3.3(3) ns from the present work is consistent with the previously reported one: 3.2(6) ns [40].

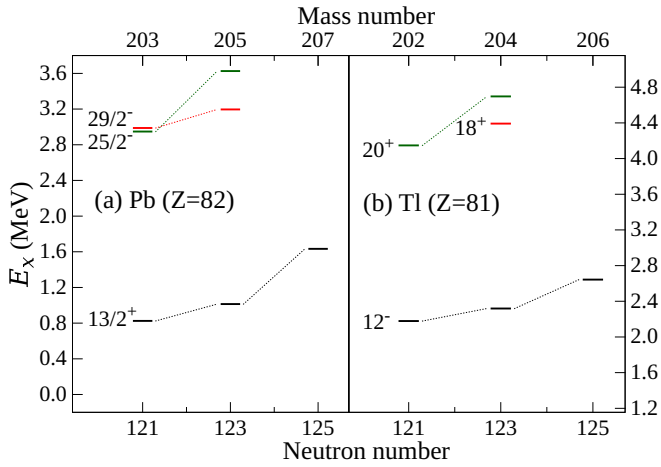

FIG. 12. Comparison of excitation energies of key levels, most of which have isomeric character, in Tl and Pb isotopes. Different energy scales are used for the two panels of the figure in order to account for the contribution of the $h_{11/2}$ proton in the Tl case.

$N = 121$ ^{201}Hg and ^{203}Pb, and $N = 123$ isotones ^{203}Hg and ^{205}Pb, respectively [9,33]. The increase in the 12^- energy from ^{202}Tl to ^{206}Tl may be understood in terms of the neutron Fermi level moving farther away from the $i_{13/2}$ orbital, a situation similar to that invoked in the case of the 7^+ state. The absence of isomeric character for the 12^- level in ^{202}Tl may then be attributed to the available 134-keV $E1$ decay path. In comparison, the lowest multipolarity for the transitions deexciting the 12^- isomers in ^{204}Tl and ^{206}Tl are $E3$ and $M4$ ones, respectively, leading to the observed isomerism.

In ^{202}Tl, the following four-nucleon configurations may be expected to exhibit isomeric character: $\pi h_{11/2}^{-1} \otimes \nu (i_{13/2}^{-2}, p_{1/2}^{-1})$, $\pi h_{11/2}^{-1} \otimes \nu (i_{13/2}^{-2}, f_{5/2}^{-1})$, and $\pi h_{11/2}^{-1} \otimes \nu i_{13/2}^{-3}$, and these would lead to 18^+, 20^+, and 22^- states, respectively. In ^{204}Tl, the 18^+ and 22^- states are established as isomers and decay by $M2$ or $E3$ transitions; however, the 20^+ level deexcites through a 305-keV $E2$ γ ray and, therefore, does not exhibit isomerism [1]. To gain further insight, it is useful to consider two-neutron states in neighboring even-A Pb isotopes, where the above mentioned orbitals are involved through the $\nu(i_{13/2}^{-1}, p_{1/2}^{-1})$ and $\nu(i_{13/2}^{-1}, f_{5/2}^{-1})$ configurations leading to 7^- and 9^- states [34,35]. These have been established to be of isomeric character, with the exception of the 9^- level in ^{206}Pb [36]. The energy separation between these levels in ^{202,204}Pb is small (<80 keV), with the 7^- state lying above the 9^- one [34,35]. The comparison can be extended by including four-neutron states in ^{202}Pb and ^{204}Pb, arising from the $\nu(i_{13/2}^{-3}, p_{1/2}^{-1})$ and $\nu(i_{13/2}^{-3}, f_{5/2}^{-1})$ configurations, leading to the 17^- and 19^- levels, respectively [34,35]. In ^{202}Pb, the 17^- level lies just below the 19^- state (though the precise value of the energy difference is not known), while in ^{204}Pb, it is lower in energy by 434 keV. It is, therefore, expected that the four-nucleon, 18^+ and 20^+ states in ^{202}Tl would be close in excitation energy. It is evident, from the results obtained in the present work, that the 18^+ level must be located slightly higher in energy than the 20^+ state, and that, therefore, the only available decay path proceeds to the 17^- level via an $E3$ transition of 286 keV. This situation in turn leads to the long-lived, 215(10) μs isomer. Based on the considerations listed above, the $\pi h_{11/2}^{-1} \otimes \nu(i_{13/2}^{-2}, f_{5/2}^{-1})$ configuration is assigned to the 20^+ isomer in ^{202}Tl. It is expected that both the 18^+ and 22^- levels lie above the isomer; however, their decay could not be observed in the present data due to the long-lived nature of the 20^+ state itself. No transition decaying to the 17^- level from a possible 18^+ state was observed.

B. Empirical and shell-model calculations

As already alluded to above, the newly observed excited states in ^{202}Tl result from intrinsic excitations. In order to understand their nature, particularly that of the isomeric states, two approaches have been employed. First, empirical calculations were carried out using single-nucleon energies from neighboring nuclei, and residual interactions for different configurations derived from established isomers in the region. Second, shell-model calculations were also performed. A description of both approaches is presented below.

For the empirical calculations, one-proton energies were derived from an average of the respective values in neighboring Tl isotopes; i.e., ^{201}Tl and ^{203}Tl. These values are as follows: 0 keV ($\pi s_{1/2}$), 305 keV ($\pi d_{3/2}$), and 1467 keV ($\pi h_{11/2}$). The $\nu i_{13/2}$ energy for ^{202}Tl has been adopted as the average of the respective energies in the $N = 121$ isotones, ^{201}Hg (766 keV) and ^{203}Pb (825 keV). For the calculation of energies for higher-lying, four-nucleon levels located above the 12^- state in ^{202}Tl, the $\pi h_{11/2}$ energy has been added to those energies of appropriate three-neutron states (mostly isomeric ones) in Pb isotones with residual interactions incorporated as described below. The magnitude of the residual interactions for specific configurations was obtained by inspecting isomeric configurations in ^{204}Tl and its isotone, ^{205}Pb. Since the residual interactions are specific to a given configuration, these values were directly adopted for ^{202}Tl. The values of these interactions obtained using this procedure are as follows: 7^+ (131 keV): $\pi s_{1/2}^{-1} \otimes \nu i_{13/2}^{-1}$; 12^- (-121 keV): $\pi h_{11/2}^{-1} \otimes \nu i_{13/2}^{-1}$; 18^+ (-271 keV): $\pi h_{11/2}^{-1} \otimes \nu(i_{13/2}^{-2}, p_{1/2}^{-1})$; 20^+ (-395 keV): $\pi h_{11/2}^{-1} \otimes \nu(i_{13/2}^{-2}, f_{5/2}^{-1})$; 22^- (-389 keV): $\pi h_{11/2}^{-1} \otimes \nu i_{13/2}^{-3}$. The empirical energies in Fig. 13 have been obtained using the above mentioned procedure. Similar calculations for ^{203}Pb yielded the following results: (a) $25/2^-$ state [$\nu(i_{13/2}^{-2}, p_{1/2}^{-1})$]: $(E_x)_{cal} = 3008$ keV compared to $(E_x)_{exp} = 2923.4 + x$ keV; (b) $29/2^-$ state [$\nu(i_{13/2}^{-2}, f_{5/2}^{-1})$]: $(E_x)_{cal} = 3002$ keV compared to $(E_x)_{exp} = 2949.2$ keV. Such a calculation could not be performed for the $I^\pi = 37/2^+$ state in ^{203}Pb on account of the limited experimental information.

Shell model calculations using the KHH7B [37] effective interaction have been performed for ^{202}Tl. This interaction was originally developed for proton orbitals $d_{5/2}$, $h_{11/2}$, $d_{3/2}$, and $s_{1/2}$ below the $Z = 82$ gap, and the $h_{9/2}$, $f_{7/2}$, and $i_{13/2}$ ones above it, and for neutron orbitals $i_{13/2}$, $p_{3/2}$, $f_{5/2}$, and $p_{1/2}$ below the $N = 126$ gap, and the $g_{9/2}$, $i_{11/2}$, $j_{15/2}$ states above it. In our calculations, we have not allowed proton excitations across the $Z = 82$ shell and neutron ones across the $N = 126$ one. Thus, the active orbitals in our shell model calculations for protons are $d_{5/2}$, $h_{11/2}$, $d_{3/2}$, and $s_{1/2}$, and for neutrons are

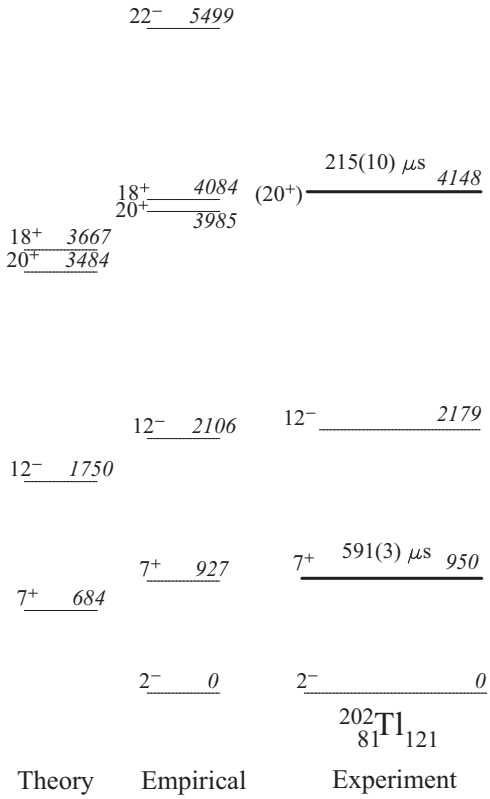

FIG. 13. Excitation energies of selected states in ^{202}Tl from experiment, empirical and shell-model (theory) calculations. Details are provided in the text.

$i_{13/2}$, $p_{3/2}$, $f_{5/2}$, and $p_{1/2}$. The shell-model code OXBASH [38] was used for the diagonalization of the matrices of interest.

A comparison of the empirical and shell-model calculations with the experimental data (Fig. 13) leads to the following conclusions. The empirical calculations exhibit, as expected, good agreement with the experimental data, and also serve to validate the proposed configuration assignments. The two- and four-nucleon energies from empirical calculations agree to within 80 and 160 keV, respectively, with the data. The deviations between the values from shell-model calculations and experiment are, however, much larger: 266 and 429 keV for two-nucleon, and 664 keV for four-nucleon states. Both empirical and shell-model calculations predict a lower excitation energy for the 20^+ state in comparison to the 18^+ level, as observed in the experiment.

C. New isomer in ^{203}Pb

The new isomer, with $T_{1/2} = 2.5(3)$ ns and $I^\pi = 37/2^+$, in ^{203}Pb is associated with a five-neutron excitation since the highest spin that can be realized from three neutrons is only $33/2\,\hbar$ ($\nu i_{13/2}^{-3}$). The configuration for this $37/2^+$ isomer is assigned as $\nu(i_{13/2}^{-3}, f_{5/2}^{-1}, p_{1/2}^{-1})$ with a possible admixture from the $\nu(i_{13/2}^{-3}, p_{3/2}^{-1}, p_{1/2}^{-1})$ excitation. The former configuration may have a greater contribution based on the observation, in ^{203}Pb, of three-neutron isomers with $I^\pi = 25/2^-$ and $29/2^-$ from the excitation of two $i_{13/2}$ neutrons, and a $p_{1/2}$ and $f_{5/2}$ neutron, respectively. The isomeric character of the $37/2^+$ state is most likely due to the configuration hindrance involved in the transition from a level with a purely five-neutron character to one of predominant three-neutron nature.

D. Transition probabilities

The partial half-lives for γ-ray decays from isomers in the $N = 121$ isotones ^{202}Tl and ^{203}Pb, and the $N = 123$ ^{204}Tl and ^{205}Pb ones, and their comparison with Weisskopf single-particle estimates, are presented in Table IV. It is evident that, for $E2$ and $E3$ multipolarities, the transition rates from experiment are almost within an order of magnitude of the single-particle estimates, as expected for deexcitation from states with intrinsic character. The transition rates for $M2$ decays in ^{204}Tl and ^{205}Pb are, however, hindered by about three orders of magnitude. This feature extends to other $M2$ decays in this region and will be addressed in a subsequent publication [39].

V. SUMMARY

The high-spin level structure of ^{202}Tl has been studied using the INGA and Gammasphere arrays. The decay scheme of ^{202}Tl has been extended from $I^\pi = 10^+$ to $I^\pi = 20^+$ with the identification of a new $T_{1/2} = 215(10)$ μs isomer, originating from a four-nucleon excitation. Fifteen new transitions have been added to the level scheme. The half-life of the

TABLE IV. Decays of isomeric states in selected Tl and Pb isotopes and comparison with Weisskopf estimates. Isomers which are newly identified from the present work are indicated with an asterisk (∗). The others were previously established [1,9,22].

Isotope	I_i^π	$T_{1/2}$ (s)	E_γ (keV)	Mult. ($E\lambda$)	$T_{1/2}^\gamma$ (s)	$T_{1/2}^W$ (s)	$B(E\lambda)$ W.u.
^{202}Tl	7^+	5.91×10^{-4}	460	$E3$	6.6×10^{-4}	1.1×10^{-4}	0.17
	20^+	2.15×10^{-4}∗	286	$E3$	3.7×10^{-4}	3.1×10^{-3}	8.38
^{203}Pb	$37/2^+$	2.5×10^{-9}∗	568	$E2$	2.6×10^{-9}	1.3×10^{-10}	0.05
^{204}Tl	7^+	6.2×10^{-5}	690	$E3$	6.4×10^{-5}	6.4×10^{-6}	0.10
	18^+	4.2×10^{-7}	754	$M2$	1.2×10^{-6}	3.7×10^{-9}	3.08×10^{-3}
			1036	$E3$	6.9×10^{-7}	3.7×10^{-7}	0.54
^{205}Pb	$33/2^+$	6.3×10^{-8}	97	$E2$	1.3×10^{-6}	9.0×10^{-7}	0.69
			1252	$E3$	5.8×10^{-7}	9.8×10^{-8}	0.17
			1536	$M2$	1.3×10^{-7}	1.1×10^{-10}	0.85×10^{-3}

$I^{\pi} = 37/2^{+}$ state in ^{203}Pb is determined to be 2.5(3) ns. While coincidence data from both experiments were useful in establishing the level scheme of ^{202}Tl, complementary aspects could be addressed using the two separate sets of data. The one from the INGA experiment contained information on low-energy γ rays, and also on DCO and IPDCO ratios for spin-parity assignments. The Gammasphere data were particularly useful for the determination of the half-lives of isomers and the inspection of threefold coincidence events. The newly identified isomers in ^{202}Tl and ^{203}Pb are assigned four- and five-nucleon $\pi h_{11/2}^{-1} \otimes \nu(i_{13/2}^{-2}, f_{5/2}^{-1})$ and $\nu(i_{13/2}^{-3}, f_{5/2}^{-1}, p_{1/2}^{-1})$ configurations, respectively. In the case of the latter, an admixture with an $\nu(i_{13/2}^{-3}, p_{3/2}^{-1}, p_{1/2}^{-1})$ excitation is probable. Excited levels in both nuclei originate from intrinsic excitations, and are well described by empirical calculations. Shell-model calculations, using the OXBASH code and the KHH7B interaction, are found to systematically underestimate the excitation energies obtained from experiment.

ACKNOWLEDGMENTS

The authors would like to thank the accelerator staff at the IUAC and ANL, and the INGA Collaboration. We also wish to thank I. Ahmad, J. P. Greene, A. J. Knox, D. Peterson, U. Shirwadkar, X. Wang, and C. M. Wilson for assistance during the Gammasphere experiment. We acknowledge financial support from the Department of Science and Technology, Government of India (Grant No. IR/S2/PF-03/2003-III) for the INGA project. S.G.W. acknowledges support from the DST-INSPIRE Ph.D. Fellowship of the Department of Science and Technology, Government of India (Fellowship No. IF150098). S.K.T. would like to acknowledge support from the University Grants Commission, India, under the Faculty Recharge Programme. S.S. acknowledges support from the DST-INSPIRE Ph.D. Fellowship of the Department of Science and Technology, Government of India (Fellowship No. IF170965). M.H. would like to acknowledge support from the University Grants Commission, India, under the Faculty Recharge Programme. This work is supported by the U.S. Department of Energy, Office of Science, Office of Nuclear Physics, under Grants No. DE-FG02-94ER40848, No. DE-FG02-94ER40834, No. DE-FG02-97ER41041 (UNC), and No. DE-FG02-97ER41033 (TUNL), and Contract No. DE-AC02-06CH11357. The research described here utilized resources of the ATLAS facility at ANL, which is a DOE Office of Science user facility.

[1] R. Broda, K. H. Maier, B. Fornal, J. Wrzesinski, B. Szpak, M. P. Carpenter, R. V. F. Janssens, W. Kròlas, T. Pawłat, and S. Zhu, Phys. Rev. C **84**, 014330 (2011).
[2] J. Wrzesinski, R. Broda, B. Fornal, W. Kròlas, T. Pawłat, M. P. Carpenter, R. V. F. Janssens, D. Seweryniak, S. Lunardi, C. A. Ur *et al.*, Eur. Phys. J. A **20**, 57 (2004).
[3] O. Häusser, J. R. Beene, T. K. Alexander, A. B. McDonald, and T. Faestermann, Phys. Lett. B **64**, 273 (1976).
[4] A. J. Kreiner, M. Fenzl, S. Lunardi, and M. A. J. Mariscotti, Nucl. Phys. A **282**, 243 (1977).
[5] E. A. Lawrie, P. A. Vymers, Ch. Vieu, J. J. Lawrie, C. Schück, R. A. Bark, R. Lindsay, G. K. Mabala, S. M. Maliage, P. L. Masiteng *et al.*, Eur. Phys. J. A **45**, 39 (2010).
[6] P. Roy, S. K. Tandel, Saket Suman, P. Chowdhury, R. V. F. Janssens, M. P. Carpenter, T. L. Khoo, F. G. Kondev, T. Lauritsen, C. J. Lister *et al.*, Phys. Rev. C **100**, 024320 (2019).
[7] M. G. Slocombe, J. O. Newton, and G. D. Dracoulis, Nucl. Phys. A **275**, 166 (1977).
[8] S. Das Gupta, S. Bhattacharyya, H. Pai, G. Mukherjee, Soumik Bhattacharya, R. Palit, A. Shrivastava, A. Chatterjee, S. Chanda, V. Nanal *et al.*, Phys. Rev. C **88**, 044328 (2013).
[9] U. Rosengard, P. Carlè, A. Källberg, L. O. Norlin, K. G. Rensfelt, H. C. Jain, B. Fant, and T. Weckström, Nucl. Phys. A **482**, 573 (1988).
[10] J. Wrzesinski, G. J. Lane, K. H. Maier, R. V. F. Janssens, G. D. Dracoulis, R. Broda, A. P. Byrne, M. P. Carpenter, R. M. Clark, M. Cromaz *et al.*, Phys. Rev. C **92**, 044327 (2015).
[11] S. Muralithar, K. Rani, R. Kumar, R. P. Singh, J. J. Das, J. Gehlot, K. S. Golda, A. Jhingan, N. Madhavan, S. Nath *et al.*, Nucl. Instrum. Methods Phys. Res. A **622**, 281 (2010).
[12] I.-Y. Lee, Nucl. Phys. A **520**, c641 (1990).
[13] R. V. F. Janssens and F. S. Stephens, Nucl. Phys. News **6**, 9 (1996).
[14] K. S. Krane, R. M. Steffen, and R. M. Wheeler, Nucl. Data Tables **11**, 351 (1973).
[15] A. Kramer-Flecken, T. Morek, R. M. Lieder, W. Gast, G. Hebbinghaus, H. M. Jager, and W. Urban, Nucl. Instrum. Methods Phys. Res. A **275**, 333 (1989).
[16] K. Starosta, T. Morek, Ch. Droste, S. G. Rohozinski, J. Srebrny, A. Wierzchucka, M. Bergström, B. Herskind, E. Melby, T. Czosnyka *et al.*, Nucl. Instrum. Methods Phys. Res. A **423**, 16 (1999).
[17] S. K. Tandel *et al.*, Phys. Lett. B **750**, 225 (2015).
[18] S. G. Wahid *et al.*, Phys. Rev. C **92**, 054323 (2015).
[19] S. K. Tandel *et al.*, Phys. Rev. C **94**, 064304 (2016).
[20] D. C. Radford, Nucl. Instrum. Methods Phys. Res. A **361**, 297 (1995).
[21] N. Frascaria, J. P. Didelez, N. S. Chant, and C. C. Chang, Phys. Rev. C **16**, 603 (1977).
[22] N. Fotiades, R. O. Nelson, M. Devlin, and J. A. Becker, Phys. Rev. C **76**, 014302 (2007).
[23] A. J. Kreiner, M. A. J. Mariscotti, C. Baktash, E. der Mateosian, and P. Thieberger, Phys. Rev. C **23**, 748 (1981).
[24] S. Bhattacharya, S. Bhattacharyya, S. Das Gupta, H. Pai, G. Mukherjee, R. Palit, F. R. Xu, Q. Wu, A. Shrivastava, Md. A. Asgar *et al.*, Phys. Rev. C **95**, 014301 (2017).
[25] T. Kibedi, T. W. Burrows, M. B. Trzhaskovskaya, P. M. Davidson, and C. W. Nestor, Jr., Nucl. Instrum. Methods A **589**, 202 (2008).
[26] H. J. Kim and W. T. Milner, Nucl. Instrum. Methods **95**, 429 (1971).
[27] S. Zhu and F. G. Kondev, Nucl. Data Sheets **109**, 699 (2008).
[28] F. G. Kondev and S. Lalkovski, Nucl. Data Sheets **108**, 1471 (2007).

[29] H. Xiaolong and K. Mengxia, Nucl. Data Sheets **133**, 221 (2016).
[30] H. Xiaolong, Nucl. Data Sheets **108**, 1093 (2007).
[31] B. Singh, Nucl. Data Sheets **107**, 1531 (2006).
[32] C. J. Chiara and F. G. Kondev, Nucl. Data Sheets **111**, 141 (2010).
[33] P. Zeyen, K. Euler, V. Grafen, C. Günther, M. Marten-Tölle, P. Schüler, and R. Tolle, Z. Phys. A **325**, 451 (1986).
[34] B. Fant, T. Weckstrom, H. C. Jain, L. O. Norlin, K.-G. Rensfelt, P. Carle, and U. Rosengard, Nucl. Phys. A **475**, 338 (1987).
[35] C. G. Linden, I. Bergstrom, J. Blomqvist, and C. Roulet, Z. Phys. A **284**, 217 (1978).
[36] J. Blomqvist, R. Liotta, L. O. Norlin, U. Rosengard, B. Fant, T. Weckstrom, H. C. Jain, and T. Lonnroth, Nucl. Phys. A **554**, 45 (1993).
[37] G. H. Herling and T. T. S. Kuo, Nucl. Phys. A **181**, 113 (1972).
[38] B. A. Brown, Oxbash for Windows, MSU-NSCL Report 1289, 2004 (unpublished).
[39] S. K. Tandel *et al.* (unpublished).
[40] H. Helppi, S. K. Saha, P. J. Daly, S. R. Faber, T. L. Khoo, and F. M. Bernthal, Phys. Rev. C **23**, 1446 (1981).